ON-BODY CHARACTERIZATION OF DUAL-BAND ALL-TEXTILE PIFAs

P. J. Soh[1, 3, *], S. J. Boyes[2], G. A. E. Vandenbosch[1], Y. Huang[2], and S. L. Ooi[3]

[1]ESAT-TELEMIC, Katholieke Universiteit Leuven, Kasteelpark Arenberg 10, Leuven 3001, Belgium

[2]RF and High Frequency Engineering Research Group, Department of Electrical Engineering and Electronics, The University of Liverpool, Brownlow Hill, Liverpool L69 3GJ, United Kingdom

[3]School of Computer and Communication Engineering, Universiti Malaysia Perlis (UniMAP), Kuala Perlis, Perlis 02000, Malaysia

Abstract—Antenna performance in terms of reflection coefficient, bandwidth, radiation pattern and efficiency is expected to be severely influenced during on-body deployment. Besides addressing the need for a systematic on-body evaluation procedure, this work presents an in-depth discussion on the measured degradation relative to free space operation. Considering a practical deployment scenario, the two antenna designs are first optimized in proximity of a human-emulating box using a commercial simulator. ShieldIt textile is chosen to build the antenna's conductive components, and this prototype is then benchmarked against another similarly-dimensioned prototype constructed using copper foil. For each material, two dual-band prototypes are fabricated, one resonating at 2.45 GHz and 5.2 GHz, and the other at 2.45 GHz and 5.8 GHz. Two realistic on-body deployment locations are chosen to be investigated, on the chest and back, considering two antenna orientations — one radiating away from the user, and the other radiating along the body. Free space and on-body reflection coefficient, bandwidth and radiation pattern are evaluated for each prototype in an anechoic chamber, while a reverberation chamber is utilized to determine their efficiency. All measurements were carried out using the same human volunteer. Evaluations show that coupling distance and conductivity are the main factors in determining efficiency rather than on-body location, given

that evaluations are carried out while the antenna keeps its planar form.

1. INTRODUCTION

A wearable antenna is an essential part in any Wireless Body Area Network (WBAN) application. Its electronic nodes are made flexible enough to be worn and work in the proximity of a user's body. Effective implementations of WBANs are expected to effectively contribute to advancements in emergency services, medical, military, identification, navigation, sports, etc. [1]. Among others, wearable antennas could assist medical monitoring for hospitalized, home-bound, or outpatients [2], and applied in emergency services communication and public safety support (e.g., firefighters) [3–5]. It could also provide flexibility in assisting communication in search, rescue and location-tracking alerts, especially in hazardous environments [6, 7]. There is also the possibility that it will become popular in consumer electronics in the near future, applied for communication [8], positioning and navigation for recreational purposes [9] and vehicles' collision-avoidance radars [10]. However, degradation of the antenna performance when worn on the human body has been one of the major deterrents in its successful implementation, be it in terms of frequency detuning, bandwidth reduction, and efficiency degradation or radiation distortion [11]. In other words, ideally, a wearable antenna must be designed to be immune enough for an on-body operation. Moreover, a flexible antenna made from textile is regarded as a realistic candidate due to the ergonomic properties that it is able to offer. Previous researches have mainly investigated detuning in proximity of human head and hand [12], which are not necessarily applicable in WBANs. On the contrary, prospective on-body antenna locations in WBANs are mainly concentrated on the upper torso, arms and legs. To be operable on body, minimal degradation in terms of bandwidth, reflection coefficient and efficiency has to be ensured, while keeping manufacturing simple and cost-effective. These performance parameters go hand-in-hand with determining the operation effectiveness of the antennas. They are expected to be the most affected when worn, due to the electromagnetic coupling with and absorption by the body.

Various textile antenna topologies have been proposed for use in the WBAN domain. While planar structures based on the microstrip topology are extremely popular, the earliest work in wearable antennas proposed PIFA as its topology [13]. A PIFA consists of a radiator, a ground plane, a shorting wall and a feeding probe. The existence of ground planes in PIFAs helps to avoid serious detuning in operation

close to the human user, in contrast to wired antennas. Moreover, the properties of PIFAs — compact in size and omni-directional in nature — enables ease of on-body mounting and allows reception of randomly polarized arriving signals [14]. It also eases resonance tweaking through radiator modification, shorting wall dimension and feeding position changes. A single, narrow band antenna could be enhanced to function with dual- or multi-band characteristics. Even though it might be slightly thicker than uni-layered microstrip types, recent investigations in [3, 13, 15] have used substrates of at least 3 mm in thickness to realize relatively narrowband textile antennas. Moreover, the use of thicker substrates reduces the possibility of extreme antenna bending while in operation.

This work is organized as follows. The first section is dedicated to introducing the antenna design, materials, and fabrication technique. Next, the proposed structure's fabrication tolerances are investigated using a commercial electromagnetic solver, CST Microwave Studio, including an in-depth evaluation of the antenna's on-body performance, carried out by defining a human-emulating box in proximity of the antenna under test (AUT). This is crucial to predetermine its changes when operating on-body and to establish a final design geometry. In the subsequent section, a study of the antenna's operation when mounted on a real human volunteer is analyzed and discussed, prior to our concluding remarks. The innovativeness of this work is listed as follows:

a) A method for consistent on-body evaluation is proposed. This includes the usage of a fleece jacket, sewn in with RF cables to enable fixed antenna mounting locations and minimal cable movements during reflection coefficient and radiation pattern evaluations.

b) A real human volunteer has been consistently used to investigate the antennas throughout all evaluations. Although it could be argued that antenna performance should vary according to subject's morphology, this method is by far more accurate than the utilization of fabricated human-emulating phantoms. Moreover, repeatability tests and the tool in (a) have been utilized to ensure consistency.

c) To our best knowledge, on-body efficiency measurements carried out using a reverberation chamber for an all-textile antenna have never been reported by other authors. In addition, this investigation involves the evaluation of efficiency between 2 GHz and 7 GHz, which has been proven to provide a minimal level of uncertainties, applicable for both conventional and flexible antennas [16, 17].
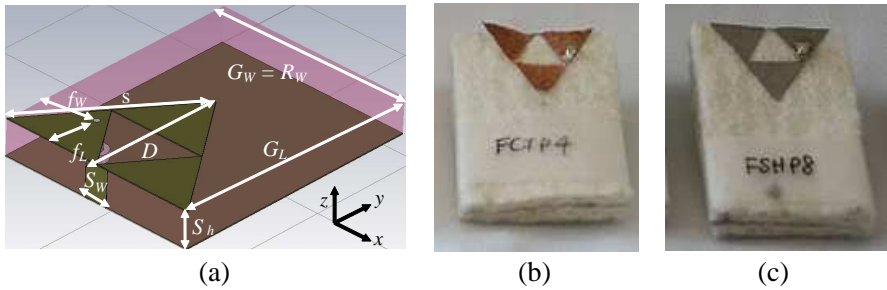
Figure 1. (a) Structure and dimensions of the proposed fractal PIFA, (b) fabricated copper foil prototype, (b) fabricated ShieldIt prototype.

2. ANTENNA TOPOLOGY

The structure of the proposed fractal PIFA consists of a radiator, a substrate, a shorting wall and a ground plane, as shown in Fig. 1. Connection of the triangular-shaped radiator to the ground plane (sized at G_L and G_w) is enabled via a shorting wall of W_w wide, centered at the base of the triangular radiator. This radiator-ground plane spacing is mechanically supported using a felt substrate with height, $h = 6$ mm, and fed using a $50\,\Omega$ SMA probe from the PIFA's ground plane. The feed is positioned at a horizontal distance of f_h and vertical distance of f_v from the antenna edge. Its radiator is designed based on a triangular-shaped, first iteration Sierpinski gasket. The initial dimensions of triangle height, D and side length, R_W, are estimated by using a resonant frequency of 2.45 GHz in the following equation [18]:

$$R_W = \frac{0.52}{\sqrt{3}} \frac{c}{f_c} \delta^n - \frac{h}{\sqrt{\varepsilon_r}} \quad \text{for } n > 0 \tag{1}$$

where n is the iteration number, $\rho = \xi - 0.230735$, c is the velocity of light in free space, f_c is the desired center frequency, ξ is the triangle's height ratio between two successive iterations ($\xi = D_{(n)}/D_{(n+1)}$), δ is the scale factor, also given by $\delta = 1/\xi$, h is the thickness and ε_r the relative permittivity of the substrate. Initial calculation using $\delta = 2$, $f_C = 2.45$ GHz, $h = 6$ mm, and $\varepsilon_r = 1.45$ yields a zeroth iteration Sierpinski triangle with $R_W = 31.8$ mm. Using simple trigonometric relations, this translates into an estimated triangle height of $D = 27.5$ mm. Similarly sized G_w and R_w and the centered shorting wall enabled practical simplicity, permitting the antenna to be fabricated using a single piece of textile. Two types of material are investigated in this work, a conventional copper foil and a conductive textile. The

Table 1. Calculated and optimized dimensions for the proposed PIFA.

Dimension/Parameters	G_L	Gw	R_W	D	f_W	f_L	S_W	S_h
Calculated	NA	31.8	31.8	27.5	NA	NA	NA	6
Optimized ($P1$) (mm)	44	34	34	24	9	8.5	4	6
Optimized ($P2$) (mm)	44	30	30	23	7	8.5	4	6

utilized flexible copper foil is 0.035 mm thick (t), whereas ShieldIt is a plain woven conductive textile coated using nickel and copper with 0.17 mm thickness. The latter provides a surface resistivity (R_s) of less than 0.05 Ω/sq, and is procured from LessEMF Inc, while the former is about five times thinner relative to ShieldIt, made of annealed copper, providing reasonably homogeneous surface resistivity/conductivity and good mechanical stability.

The design steps and optimized dimensions were presented in [19]. A comparison of calculated and optimized dimensions is presented in Table 1. The substrate used in this work, felt, is chosen to enable easy integration onto users' clothing. Its permittivity and loss tangent are given in literature within the following ranges: ε_r in between 1.18 [20] and 1.45 [21] and $\tan \delta$ in between 0.004 [20] and 0.025 [15]. This illustrates that a proper measurement of felt characteristics is still an issue. In order to select the most appropriate value for our experiments, samples of 6 mm thick have been measured using an in-house developed technique based on the cavity method, yielding a relative permittivity of $\varepsilon_r = 1.45$ and, $\tan \delta = 0.044$ at 2.45 GHz. Although this loss tangent value is higher than found in literature, it seems to be consistent with many measured efficiencies, as detailed further. CST Microwave Studio is utilized to simulate this structure at the desired frequencies of 2.45 GHz and 5.20 (or 5.80 GHz). The textile is defined as a lossy metal to simplify analysis, with an estimated conductivity of $\sigma_S = 1.18 \times 10^5$ S/m for ShieldIt, using an approximate equation proposed in [22]. For copper foil, the thickness is 0.035 mm and its conductivity is taken as $\sigma_c = 5.88 \times 10^7$ S/m.

3. SENSITIVITY ANALYSIS

Any fabrication process will introduce manufacturing inaccuracies. This inaccuracy is well-characterized for standard PCB production facilities. Even though the structure is chosen intentionally simple, the employed manual fabrication process used in this work will generate larger errors, up to ca. ±0.2 mm. Thus, a dimension-performance analysis prior to fabrication is useful in understanding

and avoiding unexpectedly large variations due to the manufacturing process. Moreover, our investigation includes the prediction of antenna performance degradation due to a human body in the design stage, which is valuable, since the antenna is always meant to be used on a human user. This section analyses the contribution of two categories of antenna parameters, namely, the physical dimensions and the material properties. Physical dimension changes up to $\pm 2.0\,\text{mm}$ with respect to optimized dimensions are investigated using the CST solver, both in free space (FS) and on body (OB), as was mentioned earlier. For OB investigations, the antenna is mounted on a rectangular-shaped box dimensioned at $200 \times 200 \times 80\,\text{mm}^3$, filled with material similar to a human body ($\varepsilon_r = 53.58$ and $\sigma = 1.81\,\text{S/m}$ at $2.45\,\text{GHz}$) [23] at a starting distance of $10.3\,\text{mm}$ [24]. Note that in this investigation, unless otherwise mentioned, the parameters used for the felt substrate are $\varepsilon_r = 1.45$ and, $\tan\delta = 0.044$. Small deviations from these values will not change the qualitative conclusions derived from this sensitivity study. The parameters found to be significantly contributing to the antenna's performance are the radiator side length and height (R_w and D), shorting wall width (S_W), substrate thickness (S_h) and feeding location (f_W and f_L). Besides that, the material parameters' effect on antenna performance (relative permittivity, ε_r, conductivity, σ, and loss tangent, $\tan\delta$) is also studied by observing the $-10\,\text{dB}$ bandwidth (BW), center frequency (f_c), total efficiency (η_{tot}) and radiated efficiency (η_{rad}). BW is taken in between the $-10\,\text{dB}$ S_{11} borders, while f_c is the calculated center frequency of this BW.

In FS, the antenna's bandwidth in the lower band (LB) changes linearly with the changes in dimensions, as can be seen in Fig. 2(a). For example, the decrease of D and R_w produces an increase in BW, whereas changes in S_w (moving S_w sideways ($MovS_w$) and increasing its width (S_w)) also affect the LB-BW similarly. For OB however, the LB-BW cannot be improved by more than $250\,\text{MHz}$. This improvement is most effectively done by decreasing D or increasing S_w, respectively.

Changes of f_W and f_L seem to produce consistent BW levels in LB, ca. $350\,\text{MHz}$ for FS and $150\,\text{MHz}$ for OB. This is an advantage, considering the feed cannot be physically moved too drastically due to the limited triangular patch area. In Fig. 2(b), UB-BW is noticed to be consistently larger by about $200\,\text{MHz}$ compared to LB, both for FS and OB. The high fluctuation in BW level in FS is due to the fact that at a certain moment two sub-bands join and form a larger band, resulting in a sudden increase of BW. In free space, two parameters capable of producing a large BW in this band are D and R_w. Notice the strong contribution by f_W and S_w movements compared to the LB. However,
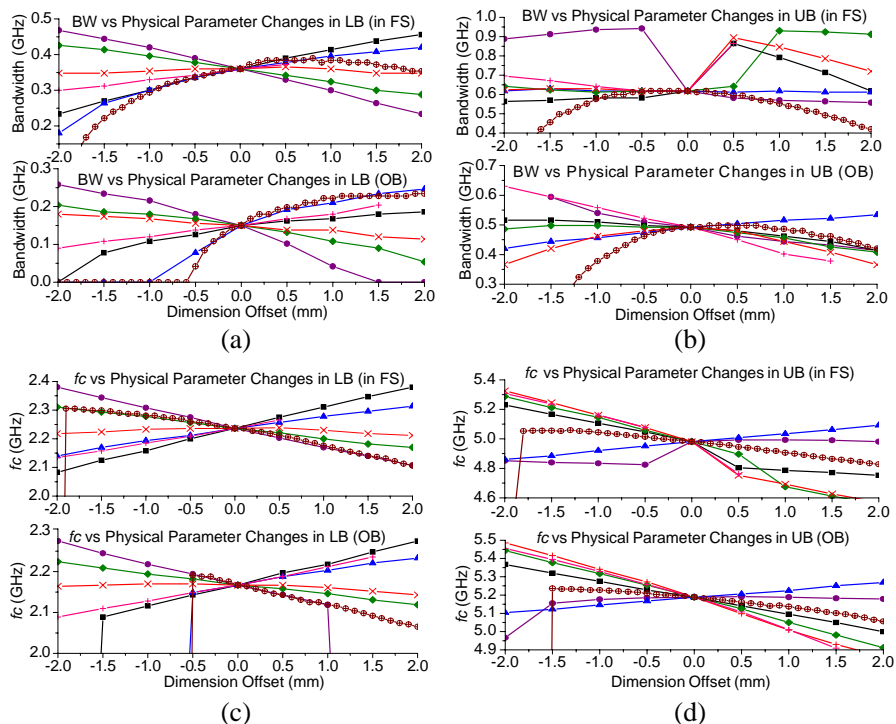
Figure 2. Center frequency (f_c) and bandwidth (BW) changes with varying physical parameters; (a-top): BW changes in LB in free space; (a-bottom): BW changes in LB on body; (b-top) BW changes in upper band (UB) in free space; and (b-bottom): BW changes in UB on body, (c-top): f_c changes in LB in free space, (c-bottom): f_c changes in LB on body; (d-top) f_c changes in upper band (UB) in free space; and (d-bottom): f_c changes in UB on body.

on body, the contribution of S_w is dampened by the loading of the body-emulating box, limiting its maximum BW to under 500 MHz. In contrast, the reduction of D is still significantly contributing to BW changes, producing a BW similar to FS cases when reduced by 2 mm. As in the lower band, the typical achievable BW within this upper band when placed on body is limited to ca. 450 MHz compared to 650 MHz in FS, a degradation of 200 MHz.

f_c behaves more linearly and conforms to conventional antenna theory. In general, it can be seen in Figs. 2(c) and (d) that body placement presents a 100 MHz downwards shift in LB, and a 200 MHz

upwards shift in UB, respectively. This is an interesting observation, since the effect of a body on textile antennas has been mostly analyzed in a single band, with the general conclusion that on body placement moves an antenna's f_c either upwards or downwards. In LB (Fig. 2(c)), the increase in R_w and D enlarges the antenna's electrical length, producing a lower f_c. Enlarging S_w and moving it away from the feed location ($MovS_w$), on the other hand, invokes an upwards f_c shift in free space. f_W movement sideways is not significant for changing f_c, but the antenna's electrical length is changed when f_L is moved closer to S_w, shifting f_c upwards, due to the creation of a shorter current path. When evaluated on body, the LB's change rate due to parameter variations is generally dampened, with an obviously lower nominal f_c. Moving S_w towards the feed and decreasing its width is seen to change the surface current to the extent that it will not produce any $-10\,\mathrm{dB}$ BW. The same can be seen when increasing D by more than 1 mm, which is shown by the abrupt drop in f_c towards zero in Fig. 2(d) (bottom). However, such drop towards zero is nowhere to be found in Fig. 2(c), even on body. Moreover, the effect of OB placement is not seen to affect the antenna's performance in UB, except for the 200 MHz difference in nominal f_c. However, contrary to LB, increments to the feed positions (f_L and f_W) are seen to be as influential as R_W and $MovS_w$ in altering f_c in UB. For both LB and UB, an S_h increment causes f_c to shift downwards with a slight BW increase. On the contrary, its decrease results in a poor matching and may easily cause non-resonance. A smaller S_h change OB also causes significant BW and f_c changes compared to in FS.

The behavior of PIFAs when varying material parameters is given in Fig. 3. In Figs. 3(a) and (b), the η_{rad} for FS and OB consistently show a difference of ca. 35% when changing $\tan\delta$ or ε_r. From another perspective, this also reflects the expected amount of η_{rad} degradation due to body absorption. A similar amount of degradation is also observed for η_{tot} in LB with increasing $\tan\delta$, which is about 10% lower than η_{rad}. However, for an increasing ε_r, η_{tot} behaves differently compared to η_{rad}, due to its tendency to affect impedance matching. For UB, the difference between η_{rad} and η_{tot} is noticeably less compared to LB for both ε_r and $\tan\delta$ changes. In free space, values of ε_r between 1.2 and 1.35 provide a very good match so that η_{rad} and η_{tot} are similar. Although smaller, such a region also exists when the PIFA is placed on body, with an ε_r between 1.35 and 1.45. Note that a change in $\tan\delta$ affects η_{rad} and η_{tot} less significantly in UB compared to LB. A maximum η_{rad}-η_{tot} difference of 5% in FS and less than 3% OB is observed with increasing $\tan\delta$, which indicates a good impedance match in UB. Such trend is also noticed when analyzing the effect of
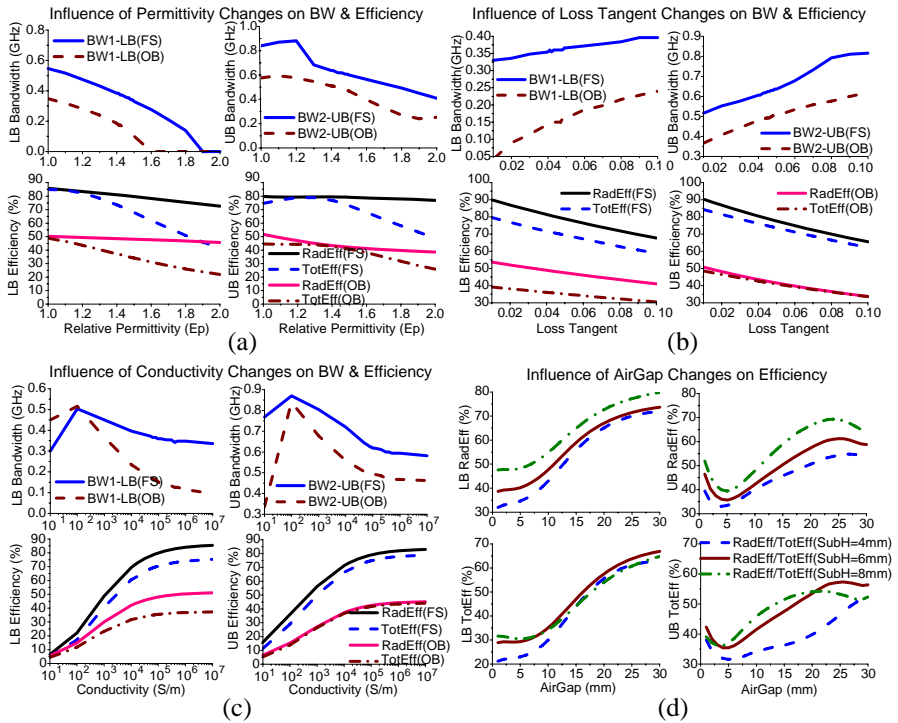
Figure 3. Bandwidth (BW) and efficiency (η_{rad}, η_{tot}) changes with varying material parameters; (a) relative permittivity (ε_r); (b) loss tangent ($\tan\delta$); (c) conductivity (σ); and (d) air gap for different S_h.

a changing σ in Figs. 3(c) and (d). η_{rad} is consistently at 85% in FS and 50% OB, while η_{tot} is 15% lower in both cases, when increasing σ from 1×10^4 to 1×10^7 S/m in LB. As was previously seen for $\tan\delta$, the η_{rad}-η_{tot} difference when σ is varied is reduced dramatically in UB — down to 5% and 3% for FS and OB, respectively. Conductivity levels of more than 1×10^4 S/m are sufficient to minimize η_{rad} and η_{tot} changes, as was also reported in [25].

The effect of the mounting distance from the body is important. Air gap (AG) refers to the distance between the PIFA's ground plane and the body model in the simulations, and is varied between 1 mm and 30 mm for three S_h sizes (4 mm, 6 mm, and 8 mm). Obeying conventional coupling theory, efficiency is worst between AG = 1 mm and AG = 5 mm, producing $\eta_{rad} < 40\%$ and $\eta_{tot} < 30$ % in LB for $S_h = 6$ mm. This 10% η_{rad}-η_{tot} difference is consistent throughout all AG variations, as efficiency increases with separation distance.
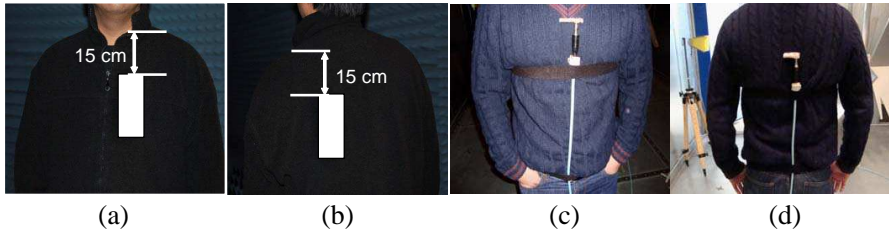
Figure 4. On body mounting locations: (a) on chest (CH10 & CV10), (b) on back (BH10 & BV10), (c) on chest (CH0) and (d) on back (BH0).

Interestingly for UB, an AG variation from $1\,\mathrm{mm}$ to $5\,\mathrm{mm}$ produces a degrading η_{rad} and η_{tot}, from 40% down to 35%. The efficiency starts to increase thereafter, similar to LB, except with a significantly smaller η_{rad}-η_{tot} difference. As expected, a thicker S_h enables better efficiencies, as seen in Fig. 3(d). η_{rad} for $S_h = 4\,\mathrm{mm}$ approaches the efficiencies of $S_h = 6\,\mathrm{mm}$ when AG $> 20\,\mathrm{mm}$, validating the fact that the antenna decouples when worn further away from the body. This analysis shows that changes to R_W, D, S_h and S_w invoke changes to BW and f_c, according to electrical length-resonance theory. Movements of f_W, f_L and S_w also provide a means for impedance matching due to the altered surface current. Changes are more linear in the LB region compared to UB, and the tuning capability for the antenna is seen to be more limited when placed on body in LB. On the other hand, for UB, impedance matching and tuning are more effective when using f_L, f_W and $MovS_w$ changes, due to the shorter available current path to enable resonance at the higher frequency. Placement on the body is expected to lower both η_{rad} and η_{tot} by about 35% to 40%. Conductivity change is seen to have minimal effect on the antenna efficiency, f_c and BW once the conductivity is larger than $1 \times 10^4\,\mathrm{S/m}$. Increasing the loss tangent introduces a maximum 15% η_{rad} and η_{tot} degradation when varied by a factor of 10, smaller in UB compared to LB. The antenna's mounting distance from the body introduces a strong coupling to the body, bringing η_{rad} down to 40% at $1\,\mathrm{mm}$, improving and approaching the FS η_{rad} when placed at several wavelengths away.

4. RESULTS AND DISCUSSION

In this investigation, two dual band designs are presented — the first prototype ($P1$) is designed to resonate at $2.45\,\mathrm{GHz}$ and $5.2\,\mathrm{GHz}$, while the second ($P2$) is designed to resonate at $2.45\,\mathrm{GHz}$ and $5.8\,\mathrm{GHz}$,

respectively. For $P1$, PIFAs from each of the materials were fabricated, and the prototypes are named according to material used — ShieldIt (SHP1), and copper foil (CTP1), and similar for $P2$. A systematic, manual fabrication process is employed, as described in [24], and constructed antennas are shown in Figs. 1(b)–(c). To maintain consistent antenna mounting location and cable routing, a custom designed fleece jacket, routed with sewn-in RF cables is utilized. Two 40 cm Huber Suhner cables are mounted vertically on the jacket on the front and back, connected to the antenna under test (AUT) at one end, and to the Network Analyzer at the other end. Two antenna locations are tested on the upper human torso: on the chest and back. To ensure the precision of the placement, two holes were created 15 cm horizontally and vertically from the top edge of the jacket. Measurements were carried out in an anechoic chamber using a male human subject, of height 178 cm and 90 kg.

Since the proposed antennas are designed to be worn, it is inevitable that the antenna should be evaluated on the upper human torso. This evaluation is carried out considering several aspects, i.e., mounting on different body locations, antenna orientations, and antenna distances from the body. Four configurations are selected on two body locations, i.e., the chest and the back, both placed on the left hand side, as shown in Figs. 4(a) and (b). For each location, the antennas are tested in both vertical and horizontal settings, mounted 10.3 mm from the body with the radiator facing outwards, away from the body. These setups are named CH10, CV10, BH10 and BV10. Besides the user's preference factor — whether he/she is more comfortable in tighter/looser clothing — the choice of the chest and back for this evaluation enabled the definition of two locations with distinct amount of gaps. In other words, clothes are relatively closer to the chest and slightly distant from the back when a user is standing or walking, for instance. With the additional clothing worn under a jacket, we reasoned that a 10.3 mm gap would be a realistic implementation, and thus chosen for evaluation. Taking into account the possibility of a change in orientation caused by movement of the user, another two additional configurations are introduced to simulate a worst case of this scenario: the antenna facing upwards, with the substrate touching the user's clothing, both on the chest and back, named CH0 and BH0, respectively, shown in Figs. 4 (c) and (d).

It can be seen from Table 2, Figs. 5 and 6 that the simulated reflection coefficient (S_{11}) is in a good agreement with measurements in free space. In simulations, CTP1 PIFAs produce 450 MHz of BW in the lower band (LB) and 730 MHz in the upper band (UB). On the other hand, SHP1 produces a lower LB and UB BW of 360 MHz
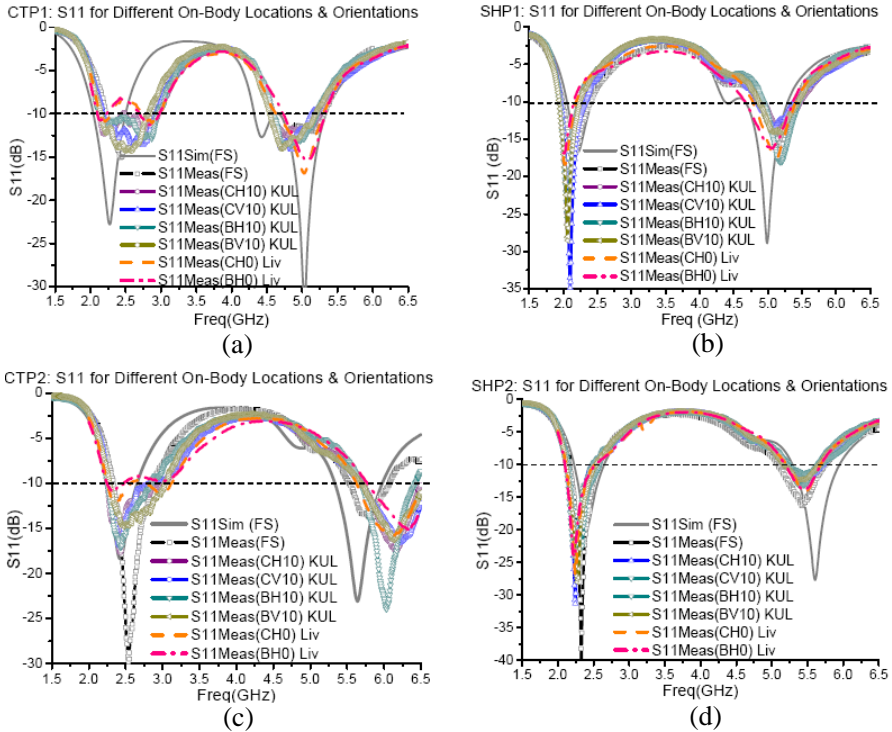
Figure 5. Simulated and measured S_{11} in free space and on-body for (a) Copper foil PIFA Prototype 1 (CTP1); (b) ShieldIt PIFA Prototype 1 (SHP1); (c) Copper foil Prototype 2 (CTP2); and (d) ShieldIt PIFA Prototype 2 (SHP2). Legend: *KUL*: measured at KU Leuven, *Liv*: measured at The University of Liverpool.
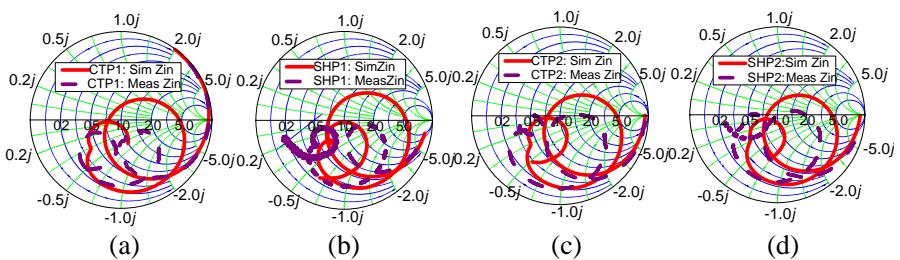

Figure 6. Simulated and measured input impedance locus for: (a) CTP1; (b) SHP1; (c) CTP2; and (d) SHP2.

Table 2. Simulated and measured bandwidth (BW) and center frequency (f_c) in free space and on body.

Antenna	Band	Parameters	FS Sim	FS Meas	CH10	CV10
CTP1	LB	BW (MHz)	450.0	575.0	837.5	743.8
		f_c (GHz)	2.27	2.48	2.54	2.56
	UB	BW (MHz)	730.0	731.3	637.5	543.8
		f_c (GHz)	4.95	4.88	4.94	4.86
SHP1	LB	BW (MHz)	366.0	325.0	275.0	350.0
		f_c (GHz)	2.24	2.14	2.09	2.14
	UB	BW (MHz)	618.0	563.0	543.8	537.5
		f_c (GHz)	4.98	5.28	5.21	5.12
CTP2	LB	BW (MHz)	402.0	550.0	775.0	556.3
		f_c (GHz)	2.46	2.61	2.64	2.55
	UB	BW (MHz)	636.0	530.0	781.3	825.0
		f_c (GHz)	5.66	5.81	6.11	6.09
SHP2	LB	BW (MHz)	420.0	412.5	412.5	437.5
		f_c (GHz)	2.44	2.37	2.34	2.36
	UB	BW (MHz)	654.0	643.8	493.8	462.5
		f_c (GHz)	5.62	5.41	5.44	5.47
Antenna	Band	Parameters	CH0	BH10	BV10	BH0
CTP1	LB	BW (MHz)	153.1	806.3	668.8	131.3
		f_c (GHz)	2.21	2.54	2.48	2.17
	UB	BW (MHz)	668.8	612.5	643.8	603.1
		f_c (GHz)	4.96	4.90	4.87	5.03
SHP1	LB	BW (MHz)	184.4	287.5	300.0	153.1
		f_c (GHz)	2.09	2.09	2.09	2.08
	UB	BW (MHz)	631.3	518.8	568.8	696.9
		f_c (GHz)	5.10	5.20	5.15	5.02
CTP2	LB	BW (MHz)	312.5	593.8	743.8	221.9
		f_c (GHz)	2.41	2.55	2.67	2.36
	UB	BW (MHz)	909.4	743.8	825.0	881.3
		f_c (GHz)	6.08	6.05	6.09	6.22
SHP2	LB	BW (MHz)	403.1	375.0	412.5	428.1
		f_c (GHz)	2.31	2.31	2.33	2.31
	UB	BW (MHz)	471.9	443.8	487.5	503.1
		f_c (GHz)	5.45	5.47	5.41	5.44

Legend: CT = copper tape; SH = ShieldIt; Sim = simulated; FS = free space; CH = chest horizontal; CV = chest vertical; BH = back horizontal; BV = back vertical.

and 618 MHz, respectively. When measured, both copper tape (CT) antennas produce about 125 to 150 MHz additional BWs in LB. For ShieldIt (SH) antennas, a better simulation-measurement agreement is observed, where the BW difference in LB is less than 50 MHz. In UB, however, this difference is similar for both PIFAs, i.e., between 50 and 110 MHz. In terms of f_c, all of the fabricated antennas produces f_c shifts of less than 200 MHz. These differences, due to the fabrication procedure, could be improved in the future by using a mould for improving cutting accuracy.

On body measurement results show that a mounting distance of more than half a wavelength at the lowest frequency of operation (2.45 GHz) does not introduce a lot of change in terms of BW and f_c shift. SHP1, SHP2, and CTP1 PIFAs produce excellent free space (FS) and on body (OB) f_c agreement, with less than 100 MHz f_c shift in both LB and UB. For the BW, however, variations are slightly larger, with a maximum change of 220 MHz, occurring for antennas fabricated from both materials. This is mainly due to the coupling to the body and absorption of waves by the body in proximity of the antenna. Note that compared to other antenna types, this absorption is reduced, considering the ground plane which shields the antenna from the body, and the fact that the main beam is radiating away from the body.

On the other hand, CH0 and BH0 are configured intentionally to have a maximum coupling to the body, avoiding the placement of an isolating ground plane in between antenna and body. Both setups have proven to show larger effects on the BW and f_c. The BW of the CT PIFAs degraded between 345 MHz and 500 MHz in LB, while for the SH PIFAs this degradation is maximal 260 MHz, also in LB. Looking at the BW in UB, all antennas show a variation of between 100 MHz and 185 MHz, which is consistent regardless of the material type. A similar effect is observed in LB, where the BW degradation for BH0 is consistently higher than for CH0 for all antenna types. Concerning f_c, CT PIFAs show a larger difference of upwards shift (320 MHz for CTP1 and less than 100 MHz for CTP2 in LB). For SH PIFAs, the f_c shift is smaller compared to the CT PIFAs, between 50 and 95 MHz in LB, and between 20 and 140 MHz in UB. Once again, f_c shifts in UB show a similar behavior for all material types. However, in most cases BH0 is observed once again to produce a higher f_c shift in both LB and UB. This is mainly due to the back, which is reasonably flat and conforms to the planar antenna placed on it, enabling a larger area for wave coupling.

In general, BW and f_c differences between materials (CTP1 vs. SHP1 and SHP2 vs. CTP2) in LB and UB are small and consistent. From this investigation it can be deduced that changes are more

influenced by the frequency range rather than by the material type, due to the similarity in conductivity. At LB, due to the similarity in design frequency, less changes are seen for two antennas constructed from a similar material. f_c difference, for example, is about 25 to 45 MHz for CT PIFAs, while SH PIFAs are smaller at LB, with a maximum of 15 MHz difference. In general, placement on BH0 and CH0 did not provide significant distinction in affecting the antenna's performance at both UB and LB, and represent the case where antenna should be worst degraded in terms of BW, f_c and radiation performance.

Since mounting on the back or chest causes minimal bending, a standard planar-positioned antenna is evaluated for the radiation pattern. The simulated and measured co-polarized components for both $\varphi = 0°$ and $\varphi = 90°$ are presented in Fig. 7 for CTP1 and SHP1. Measurements were carried out using standard spherical coordinates as defined in Fig. 1(a). The same human subject and fleece jacket were utilized to maintain placement consistency in the anechoic chamber. The antenna is measured in free space before being attached to the upper torso of the human volunteer. It can be seen that in free space, simulations and measurements agree excellently, especially in LB, except that the 120° null for $\varphi = 90°$ shifts to about 140° in the measurement. Measured received power levels are slightly lower in the lower half of the hemisphere for both cuts. The main beam is directed towards $\theta = 0°$.

When placed on body, antennas are measured at positions CH10, CV10, BH10 and BV10 to evaluate co-polarization performance in both LB and UB. Note that the BH10 and BV10 radiation patterns have been flipped to enable easy comparison with chest positions, which are 180° rotated. It is obvious from the plots that body absorption is causing a significant reduction in the lower hemisphere for on-body situations. In LB, both antenna types generate a uniform pattern in the forward direction. The null at 330° for $\varphi = 90°$, which is due to the absence of radiation along the substrate directions, is also well predicted, both for CH10 and BH10. For the same cut in UB, the same nulls as in LB are seen for both CH10 and BH10. As expected, the copper foil PIFAs show the least simulation–measurement difference, due to the conductor purity/homogeneity and mechanical robustness, compared to the textile antennas. Notice that on-body received amplitudes for textile antennas are lower compared to the copper foil, also for this reason. In addition, the radiation pattern for CTP1 is more uniform for CH10 and BH10 compared to SHP1 in both LB and UB. In UB, a portion of the high frequency signal which travels along the body's surface is gathered from the antennas' sides.

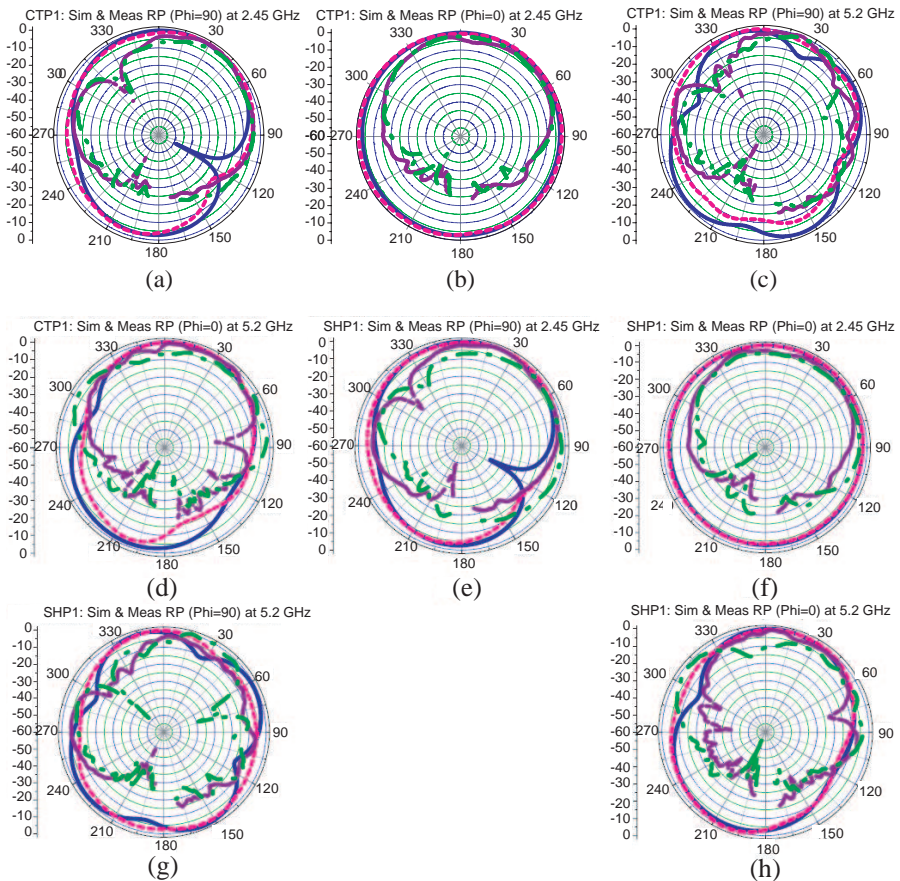The radiated power absorbed by a lossy dielectric body in the

Figure 7. Simulated and measured radiation pattern in free space and on body for: (a) CTP1 $\varphi = 90°$ at 2.45 GHz, (b) CTP1 $\varphi = 0°$ at 2.45 GHz, (c) CTP1 $\varphi = 90°$ at 5.2 GHz, (d) CTP1 $\varphi = 0°$ at 5.2 GHz, (e) SHP1 $\varphi = 90°$ at 2.45 GHz, (f) SHP1 $\varphi = 0°$ at 2.45 GHz, (g) SHP1 $\varphi = 90°$ at 5.2 GHz, (h) SHP1 $\varphi = 0°$ at 5.2 GHz. Legend: (Blue, Solid): Simulated in FS; (Pink, Dash): Measured in FS; (Green, Dash Dot): Measured for BH10; (Purple, Short Dash): Measured for CH10.

proximity of an operating antenna is expected to severely degrade its functionality. Thus, one important decider in justifying the operational capability of a wearable textile antenna is to evaluate its worn efficiency. This has been carried out using a reverberation chamber (RC), available at the University of Liverpool, sized at 3.6 ×

5.8 × 4 meters. An isotropically-stirred environment is created using a variety of stirring method, i.e., mechanical, polarization, position and frequency stirring. The RC is also sufficiently large to house the same human volunteer, with the antenna attached to his chest or back during measurements. The AUT connected to a rigid cable is attached to the volunteer using velcro ties using setups BH0 and CH0, to determine their worst-case efficiency. Throughout the measurement sequences all antennas and loading (AUT, reference antenna and human subject) were located in the "calibrated area" of the chamber. This is an area in which a statistically uniform and isotropic field distribution has been theoretically and practically demonstrated to exist. This area is situated $\lambda/2$ from the side and back walls of the chamber and also a similar distance from the mechanical stirring paddles in the chamber. The quantity λ here, it should be noted, corresponds to wavelength at the chamber's lowest usable frequency, not the free space wavelength. Further, during the measurement sequences, the human subject with AUT attached was sufficiently separated from the reference antenna at all times to avoid any coupling issues that may corrupt any average transfer power levels.

For the radiated efficiency, we refer to the IEEE definition of total radiated power to net power accepted by the antenna at its terminals. According to RC measurement procedures it can be determined by averaging the transmission coefficient $|S_{21}|$ incorporating many stirring increments and mechanisms (in our case we have used 5 degree mechanical stirring, polarization stirring and 5 position stirring; a total of 710 measured samples per frequency point have been used to form the average values). A reference antenna with known efficiency values is required for "calibration" purposes, thus via the ratio of the average power transfer functions from the reference antenna and any AUT, the unknown efficiency can be deduced from (2).

$$\eta_{RAD} = \left\{ \frac{\langle |S_{21AUT}^2| \rangle}{\langle |S_{21REF}^2| \rangle} \times \frac{1 - (|S_{11REF}^2|)}{1 - (|S_{11AUT}^2|)} \right\} \times \eta_{REF} \qquad (2)$$

where η_{RAD} is the antenna radiated efficiency, AUT the antenna under test, REF the reference antenna, η_{REF} the known radiated efficiency of the reference antenna, S_{21} = transmission coefficient, S_{11} = reflection coefficient, and $\langle \rangle$ signifies the average of the scattering parameters comprising many measurement samples from the mode stirring mechanisms employed. It should be noted that the omission of the average in the S_{11} values in (2) is because these quantities were acquired in an anechoic chamber; if determined in an RC then the S_{11} quantities should be signified as an average from the mode stirring mechanisms that are utilized. With respect to the S_{11} measurements,

both the free space and on body S_{11} were re-evaluated at the University of Liverpool in an anechoic chamber and were found to be consistent with the previous measurements carried out at KU Leuven [16] signifying that both measurements were consistent with one another, diminishing the prospect of any measurement irregularities.

To determine repeatability, a three-run CTP1 measurement was performed using setup BH0. The maximum difference of less than 2.5% for both η_{rad} and η_{tot} between the runs, as shown in Fig. 8(a), confirms the validity and stability of the measurement setup and procedure. In free space, CTP1 is highly efficient, producing slightly more than 85% for both η_{rad} and η_{tot} at 2.45 GHz, agreeing with simulations. The high efficiency is also seen at 5.2 GHz, with values ranging from

Table 3. Simulated and measured radiated (η_{rad}) and total efficiency (η_{tot}) in free space and on body.

Antenna	Band	FS Sim		FS Meas	
		η_{rad} (%)	η_{tot} (%)	η_{rad} (%)	η_{tot} (%)
CTP1	LB	84.8	79.4	87.8	85.2
	UB	82.7	80.0	85.4	81.9
SHP1	LB	80.3	70.8	70.8	70.6
	UB	79.3	75.1	75.4	73.2
CTP2	LB	86.2	84.8	83.7	80.3
	UB	77.8	63.7	85.6	78.8
SHP2	LB	81.8	80.6	79.5	76.8
	UB	73.9	62.8	78.3	67.0
Antenna	Band	CH0		BH0	
		η_{rad} (%)	η_{tot} (%)	η_{rad} (%)	η_{tot} (%)
CTP1	LB	71.1	60.7	71.2	60.9
	UB	60.8	57.3	60.1	57.5
SHP1	LB	53.2	40.2	55.6	42.4
	UB	54.1	52.7	51.1	49.0
CTP2	LB	NA	NA	NA	NA
	UB	NA	NA	NA	NA
SHP2	LB	NA	NA	NA	NA
	UB	NA	NA	NA	NA

Legend: CT = copper tape; SH = ShieldIt; Sim = simulated; Meas = measured; FS = free space; CH0 = on chest (Fig. 4(c)); BH0 = on back (Fig. 4(d)); LB = lower band; UB = upper band.

82% to 86% in free space. The simulation-measurement difference is relatively small, with less than 7% difference in LB, and less than 3% in UB, as seen in Table 3. On the other hand, a lower η_{rad} and η_{tot} is seen for SHP1: 74% and 57% respectively in LB, while UB shows ca. 70% efficiencies. Albeit the larger difference, simulations also predict these efficiency values well, simulation-measurement difference of 14% and 9% is observed in LB and UB, respectively. Outside their operating bandwidths, determining the accurate radiated efficiency from measured total efficiency becomes more difficult. This confirms the hypothesis that the surface conductivity of copper, estimated to be 100 times better than the one of conductive textile, influences efficiency. This simulation-measurement similarity is also observable for CTP2 and SHP2 in free space.

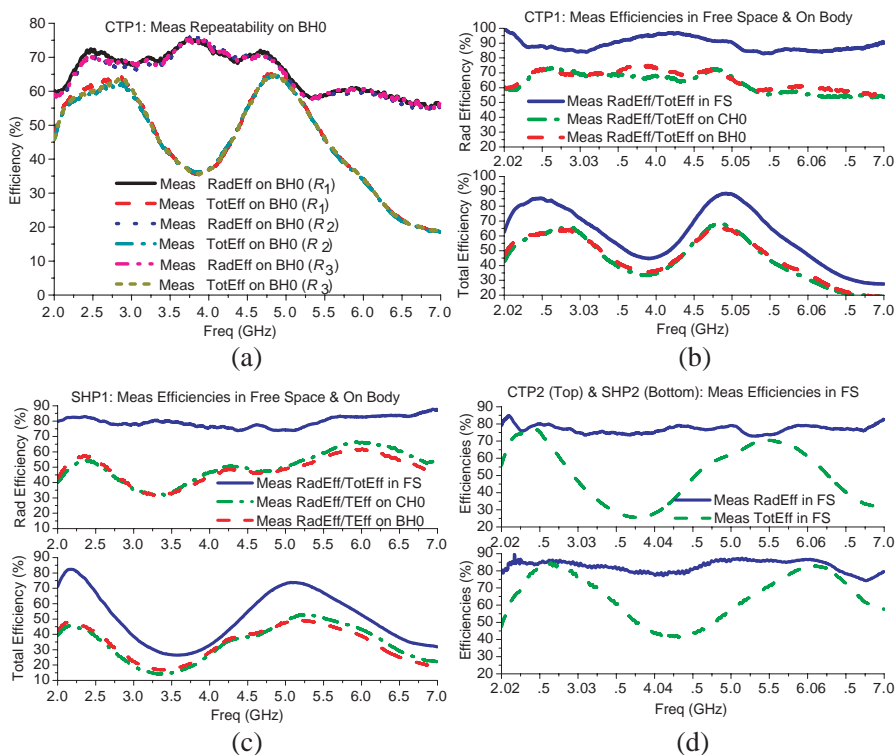Placing the antenna on body, i.e., at CH0 and BH0, an immediate

Figure 8. Efficiency measurement results in free space and on the human volunteer (a) repeatability for BH0 using CTP1, (b) η_{rad} and η_{tot} for CTP1, (c) η_{rad} and η_{tot} for SHP1, (d) η_{rad} and η_{tot} for CTP2 and SHP2.

18% to 25% efficiency drop is observed in both LB and UB for CTP1, bringing efficiencies down to between 60% and 70%, as shown in Fig. 8(b). SHP1, on the other hand, shows a lesser degree of degradation, between 17% and 21% in LB, and about 15% in UB. The better performance in UB compared to LB is mainly caused by the former's shorter wavelength, inducing a weaker antenna-to-body coupling at the higher frequency. No significant difference has been found during measurements when the AUTs are placed on the back and chest. CTP1 produced less than 1% of measured difference between CH0 and BH0, while a larger difference of 2% and 4% in LB and UB, respectively, is seen for SHP1. This implies that the coupling distance and conductivity are the main factors in determining efficiency rather than on-body location, given that evaluations are carried out while the antenna keeps its planar form. For safety regulations, specified in terms of Specific Absorption Rate (SAR), the maximum limit within Europe is 2 W/kg for every 10 grams of tissue [26]. Simulation using a Hugo human body model in CST MWS indicated that antennas placed using configuration BH0 produced 1.68 W/kg for CTP1 and 1.65 W/kg for SHP1. This is well below the safety limits, indicating the proposed antennas are safe for on-body usage.

5. CONCLUSION

A novel, compact, dual-band all-textile PIFA for wireless body area network applications is thoroughly evaluated. Simulations and measurements performed both in free space and on body indicate that the proposed textile antennas are able to operate in a dual frequency band (2.4 GHz and 5.2 GHz or 5.8 GHz), with a satisfactory reflection coefficient and bandwidth. The bandwidths are 413 MHz (LB) and 644 MHz (UB) in free space, and 440 MHz (LB) and 570 MHz (UB) when placed on body. As expected, it is seen that the coupling and absorption caused by the body reduces the antenna performance considerably for all parameters: reflection coefficient, bandwidth, radiation pattern and efficiency.

REFERENCES

1. Soh, P. J., G. A. E. Vandenbosch, X. Chen, P. S. Kildal, S. L. Ooi, and H. Aliakbarian, "Wearable textile antenna efficiency characterization using a reverberation chamber," *IEEE International Symposium on Antennas and Propagation (APURSI)*, 810–813, 2011.

2. Osman, M. A. R., M. K. A. Rahim, N. A. Samsuri, H. A. M. Salim, and M. F. Ali, "Embroidered fully textile wearable antenna for medical monitoring applications," *Progress In Electromagnetics Research*, Vol. 117, 321–337, 2011.

3. Hertleer, C., H. Rogier, L. Vallozzi, and L. Van Langenhove, "A textile antenna for off-body communication integrated into protective clothing for firefighters," *IEEE Transactions on Antennas and Propagation*, Vol. 57, 919–925, 2009.

4. Lee, E. C., P. J. Soh, N. B. M. Hashim, G. A. E. Vandenbosch, H. Mirza, I. Adam, and S. L. Ooi, "Design of a flexible minkowski-like pre-fractal (MPLF) antenna with different ground plane for VHF LMR," *International Workshop on Antenna Technology (iWAT)*, 298–301, 2011.

5. Lee, E. C., P. J. Soh, N. B. M. Hashim, G. A. E. Vandenbosch, V. Volski, I. Adam, and M. Z. A. A. Aziz, "Design and fabrication of a flexible minkowski fractal antenna for VHF applications," *5th European Conference on Antennas and Propagation (EuCAP)*, 521–524, 2011.

6. Salonen, P. and L. Hurme, "A novel fabric WLAN antenna for wearable applications," *IEEE Antennas and Propagation Society Symposium*, Vol. 2, 700–703, 2003.

7. International Cospas-Sarsat Programme, "Introduction to the cospas-sarsat system," Vol. 6, 2.1–3.5, 2009.

8. Sankaralingam, S. and B. Gupta, "Use of electro-textiles for development of wibro antennas," *Progress In Electromagnetics Research C*, Vol. 16, 183–193, 2010.

9. Rais, N. H. M., P. J. Soh, F. Malek, R. B. Ahmad, N. B. M. Hashim, and P. S. Hall, "A review of wearable antennas," *Loughborough Antennas and Propagation Conference*, 225–228, 2009.

10. Soh, P. J., G. A. E. Vandenbosch, V. Volski, and H. M. R. Nurul, "Characterization of a simple broadband textile planar inverted-F antenna (PIFA) for on body communications," *Proceedings of the 20th International Conference on Applied Electromagnetics and Communication (ICECom 2010)*, 1–4, 2010.

11. Soh, P. J., G. A. E. Vandenbosch, and J. Higuera-Oro, "Design and evaluation of flexible CPW-fed ultra wideband (UWB) textile antennas," *IEEE International RF and Microwave Conference*, 133–136, 2011.

12. Ebrahimi-Ganjeh, M. A. and A. R. Attari, "Interaction of dual band helical and PIFA handset antennas with human head and hand," *Progress In Electromagnetics Research*, Vol. 77, 225–242, 2007.

13. Salonen, P., L. Sydanheimo, M. Keskilammi, and M. Kivikoski, "A small planar inverted-F antenna for wearable applications," *Third International Symposium on Wearable Computers*, 95–100, 1999.

14. Saidatul, N. A., A. A. H. Azremi, R. B. Ahmad, P. J. Soh, and F. Malek, "Multiband fractal planar inverted-F antenna (F-PIFA) for mobile phone application," *Progress In Electromagnetics Research B*, Vol. 14, 127–148, 2009.

15. Hertleer, C., A. Tronquo, H. Rogier, L. Vallozzi, and L. Van Langenhove, "Aperture-coupled patch antenna for integration into wearable textile systems," *IEEE Antennas and Propagation Letters*, Vol. 6, 392–395, 2007.

16. Soh, P. J., S. J. Boyes, G. A. E. Vandenbosch, and Y. Huang, "Dual-band Sierpinski textile PIFA efficiency measurements," *6th European Conference on Antennas and Propagation (EuCAP)*, 3322–3326, 2012.

17. Huang, Y., Y. Lu, S. Boyes, and T. H. Loh, "Source-stirred chamber/cap method for antenna radiation efficiency measurements," *5th European Conference on Antennas and Propagation (EuCAP)*, 164–168, 2011.

18. Mishra, R. K., R. Ghatak, and D. Poddar, "Design formula for Sierpinski gasket pre-fractal planar monopole antennas," *Antennas and Propagation Magazine*, Vol. 50, 104–107, 2008.

19. Soh, P. J., G. A. E. Vandenbosch, S. L. Ooi, and M. R. N. Husna, "Wearable dual-band sierpinski fractal PIFA using conductive fabric," *Electronics Letters*, Vol. 47, No. 6, 365–367, 2011.

20. Kennedy, T. F., P. W. Fink, A. W. Chu, N. J. Champagne, G. Y. Lin, and M. A. Khayat, "Body-worn E-textile antennas: The good, the low-mass and the conformal," *IEEE Transactions of Antennas and Propagation*, Vol. 57, No. 4, 910–918, 2009.

21. Locher, I., M. Klemm, T. Kirstein, and G. roster, "Design and characterization of purely textile patch antennas," *IEEE Transactions on Advanced Packaging*, Vol. 29, No. 4, 777–788, 2006.

22. Lilja, J., P. Salonen, and P. de Maagt, "Characterization of conductive textile materials for software antenna," *IEEE Antennas and Propagation Society International Symposium (APURSI)*, 1–4, 2009.

23. Conway, G. A., W. G. Scanlon, C. Orlenius, and C. Walker, "In situ measurement of UHF wearable antenna radiation efficiency using reverberation chamber," *IEEE Wireless and Propagation Letters*, Vol. 7, 271–274, 2008.

24. Soh, P. J., G. A. E. Vandenbosch, S. L. Ooi, and N. H. M. Rais, "Design of a broadband all-textile slotted PIFA," *IEEE Transactions on Antennas and Propagation*, Vol. 60, No. 1, 379–384, 2012.

25. Soh, P. J., G. A. E. Vandenbosch, S. L. Ooi, and H. M. R. Nurul, "Characterization of a plain broadband textile PIFA," *Radioengineering*, Vol. 20, No. 4, 718–725, 2011.

26. International Commission on Non-Ionizing Radiation Protection (ICNIRP), "Guidelines for limiting exposure to time-varying electric, magnetic and electromagnetic fields (up to 300 GHz)," *Health Phys.*, Vol. 74, 494–522, 1998.